

Large-Area Free-Positioning Wireless Power Transfer to Movable Receivers

Shamsul Arefeen Al Mahmud¹, Ishtiaque Panhwar¹, and Prasad Jayathurathnage¹, *Member, IEEE*

Abstract—This article introduces a method for efficient and robust free-positioning wireless power transfer (WPT) in a large area, which can be applied to many use cases, including wireless charging of industrial robots, drones, and electric scooters. In these large areas of WPT applications, multiple transmitters (Tx) are placed in a pad-like area, and the Tx coils are optimally excited to enable robust and efficient power transfer to movable receivers within the charging area. The proposed configuration enables almost continuous magnetic flux path from a set of Tx coil(s) to another set of Tx coil(s) through the receiver coil ferrite core. Therefore, efficient power transfer is ensured throughout the whole Tx coverage area. The article introduces a novel method to detect the position and orientation of the receiver only from the Tx-side measurements. The proposed solution is experimentally verified in a laboratory prototype, and the experimental results show dc-to-dc efficiency of 91% with only 1% variation in most of the Rx positions.

Index Terms—Coil activation, free-positioning wireless charging, multi-tx wireless power transfer (WPT), robot charging.

I. INTRODUCTION

RECENTLY, there has been an increasing use of wireless power transfer (WPT) technology in various applications, such as consumer electronics [1], electric vehicle (EV) charging [2], industrial or warehouse robots [3], and unmanned aerial vehicles. This increased need of WPT technology necessitates the development of innovative methods and solutions to improve the robustness and efficiency of WPT systems.

In particular, efficient and robust WPT in a large area has become the key requirement for charging or powering freely movable receivers in many applications, including automated mobile robots, kitchen appliances, and dynamic EV charging [1]–[3]. For example, warehouse robots can be continuously recharged while they are in operation if the floor is equipped with a WPT-enabled infrastructure. Such solutions would enable

Manuscript received October 11, 2021; revised December 22, 2021; accepted January 8, 2022. Date of publication January 25, 2022; date of current version July 8, 2022. This work was supported in part by Academy of Finland Postdoctoral researcher under Grant 333479 and in part by Business Finland Research-to-business under Grant 1527/31/2020. (Corresponding author: Prasad Jayathurathnage.)

The authors are with the School of Electrical Engineering, Aalto University, 02150 Espoo, Finland (e-mail: shamsul.almahmud@aalto.fi; ishtiaque.panhwar@aalto.fi; prasad.jayathurathnage@aalto.fi).

Color versions of one or more figures in this article are available at <https://doi.org/10.1109/TIE.2022.3144591>.

Digital Object Identifier 10.1109/TIE.2022.3144591

full and continuous availability of robots without the need for work breaks for charging. Such technology reduces the onboard battery size and mitigates the need for separate charging infrastructure [4]. In case of dynamic wireless charging of EVs, the roads are electrified with WPT coils, and the vehicles are wirelessly charged on the move. For this purpose, as the vehicles move in high speed, a large wireless charging area is needed to extract considerable amount of energy.

To facilitate efficient WPT in a large area, there have been two primary proposals. 1) The use of a large transmitter (Tx) coil to cover the whole charging area [5]; and 2) The use of multiple small transmitting coils spread over the charging area [6]. The use of a large Tx coil may be relatively simpler and cost effective method to generate homogeneous electromagnetic field in a large area, however, it is not a feasible option for moderate- and high-power applications because of the following reasons: 1) unwanted electromagnetic exposure in uncoupled area, 2) low coupling, and 3) not able to control the power flow to multiple receivers. Therefore, the use of multiple Tx coils is the only feasible option to enable large-area WPT [7]–[9]. However, the cost and complexity is one of the main concerns for multi-Tx WPT systems. The key challenges in large-area multi-Tx WPT systems are robust performance and the optimal activation of Tx coils. Conventional multi-Tx WPT devices require either extra position sensors to detect receiver positions, or a data communication link to transfer measured data from Rx-side, or both. Alternatively, this article proposes an activation method for large-area multi-Tx WPT without the need for any measurements from the Rx side, which will greatly reduce the complexity of multi-Tx WPT systems.

The research focus of designing dynamic WPT systems for EV charging applications has been on achieving robust performance with respect to linear movement of the receiver [10]–[15]. For example, LCC compensation topology has been proposed to reduce the output power pulsation in dynamic WPT [10], [11]. In addition, different coil designs, namely, DD-coil [16], DDQ-coil [17], quadrature-coils [18], DQ-I-coil [12], [13] have been adopted with the goal to maintain robust power transfer against 1-D (linear movement) receiver movements. Alternatively, a combination of DD-coils and square-coils as a linear-Tx array can help to further improve the power profile along the array [14]. However, the performance of these classical coil designs suit only 1-D Rx positioning, and severely degrade if Rx devices move over an area on a 2-D surface.

There have been several attempts to enable free-positioning in 2-D space by using multi-Tx pads, to achieve homogeneous

magnetic field distribution in a large area, but activation and deactivation of multiple Tx coils to avoid unwanted exposure outside of the receiver position are still unsolved problems [19], [20]. The need for dynamic activation of coils in multi-Tx WPT systems may increase the system complexity due to the requirement of knowing the receiver position or mutual inductances between different Tx and Rx. For example, there have been several proposals to activate multiple Tx coils with the use of voltage and/or current measurements from both Tx and Rx sides [19], [21]–[23], which require an additional communication channel for data transfer from the Rx side to the Tx side. Implementation of such data communication becomes complex and tedious when there are multiple receiver devices to be charged wirelessly in the same charging area. In addition, the use of additional position detector circuits has been introduced on both Tx and Rx sides, which increases cost and complexity due to the need for multiple sensing circuits [24]. Characterization of the WPT system without any Rx-side measurements can greatly simplify the circuits, minimize costs, and increase efficiency.

There have been several proposals to characterize WPT systems without Rx-side sensors [25]–[27]. For example, in [25], [26] the fundamental harmonic components of the input current and voltage are used to estimate the load voltage or output power. One of the prerequisites of the method proposed in [25] is to know the system specifications, such as the coil inductance and parasitic resistances. However, such knowledge of the system is not always available or accurate, which can lead to measurement errors. A primary-side parameter extraction method for single Tx–Rx WPT system is proposed in [27] using a control strategy synchronized with the Rx-side converter. However, these methods become extremely complex when applied for multi-Tx WPT systems. Therefore, an effective activation method for multiple Tx coils without any receiver sensors is needed.

In this article, we introduce an alternative, counterintuitive approach, where the two nearest Tx coils are fed out of phase. In this case, the total flux created by the two coils forms a loop going from one Tx coil into the other. When the receiving coil is placed between the two Tx coils are fed in this fashion, nearly all of the flux passes through the receiver, offering high-efficiency and robust operation. With proper configuration of coil activation, this approach guarantees robust high efficiency independent of the receiver position or orientation. Note also that this configuration reduces unwanted exposure to stray magnetic flux, since the flux pipe is localized in the near vicinity of the surface and the Rx device.

In addition, we propose a simple method for activation and receiver position estimation for multi-Tx WPT systems only using Tx-side measurements. The proposed activation uses measurements from inactive coils' compensation inductors that are induced only if there is a properly tuned receiver in near vicinity. Therefore, this approach does not trigger false activation due to other disturbances, such as foreign metal objects. Main contributions of this article include the following: 1) a new method for activation and deactivation of Tx coils in a multi-Tx WPT system without a need for any measurements from the receiver side and 2) a new configuration of multi-Tx WPT systems with

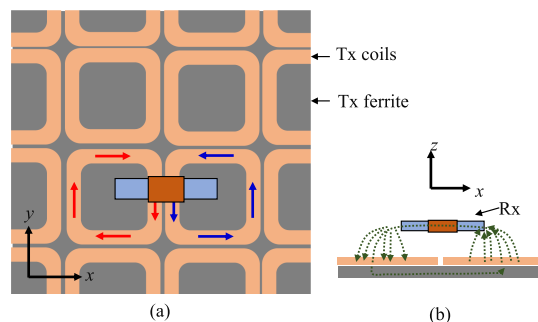


Fig. 1. Proposed multicoil arrangement to enable efficient WPT in a large area. (a) Top view. (b) Side view.

a novel type of receiver that enables full freedom of positioning in a large-area WPT setups.

The rest of this article is organized as follows. Section II introduces the proposed WPT system. Next, the system analysis with the explanations of the basis of the proposed activation strategy is presented in Section III. Next, the design and experimental prototype explanation is presented and discussed in Section IV. Then, the receiver detection and Tx activation method is discussed in Section V. Then, different experimental studies are presented in Section VI. Finally, Section VII concludes this article.

II. PROPOSED MULTICOIL WPT SYSTEM WITH LOCAL FLUX LOOPS

A. System Overview

The proposed multi-Tx WPT system is illustrated in Fig. 1. Here, multiple Tx coils cover the charging area. A set of rectangular coils together with a ferrite layer are used as Tx coils, while the Rx coil is wound around a rod-type ferrite core. We activate at least two Tx coils that are nearest to the Rx position. The currents in the active coils have the same magnitude but with a 180° phase difference. We term one of them as “*positive mode*” coil (illustrated using red arrows in Fig. 1) and the other one as “*negative mode*” coil (illustrated using blue arrows in Fig. 1). This pattern of Tx coils activation generates equal and oppositely directed magnetic fields, which facilitates magnetic flux lines coming out from one Tx coil (e.g., the *positive mode* coil) to go to the other one (e.g., the *negative mode* coil) through the Rx coil [refer to Fig. 1(b)]. All the coils that are not activated are referred to as *inactive mode* Tx with zero coil currents. Depending on the position of the receiver, different Tx configurations can be activated, which is discussed in detail in the following sections.

The main difference as compared to conventional multicoil configurations is that the out-of-phase configuration of currents in each coil pair strongly enhances the flux flow through the receiver, since the two Tx and the receiver form an effective loop conductor for magnetic flux. Next, the implementation of all three modes and the proposed position detection method without using any receiver-side measurements are explained.

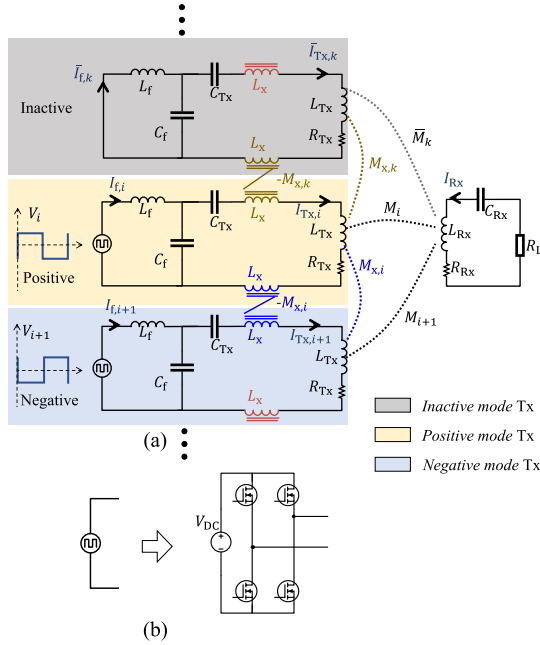


Fig. 2. (a) Equivalent circuit of a multi-Tx WPT system with *positive* mode, *negative* mode, and *inactive* Tx. (b) Illustration of a full-bridge inverter as the power source.

B. Tx Configurations

The equivalent circuit representation of the proposed WPT system is shown in Fig. 2. First, LCC compensation is chosen to realise constant current driven Tx coils. Each Tx circuit is connected to an independent full-bridge inverter, and the Rx coil is compensated using a series capacitor. In order to cancel the crosscoupling between Tx coils, coupled inductors have been used in-series with the Tx coils, whose mutual inductances are equal to the respective crosscoupling inductances, but have the opposite signs [15]. The three modes of possible Tx coil configurations that can be set at a given time (refer to Fig. 2) can be further explained as following.

- 1) *Positive mode* Tx: The inverter connected to this Tx is working as a phase-shifted full-bridge inverter. The output voltage of this inverter and the current through its Tx coil are taken as a reference.
- 2) *Negative mode* Tx: The inverter connected to this Tx is working as a phase-shifted full-bridge inverter, but with a 180° phase difference with respect to the voltage of the *positive mode* inverter. The current through this Tx coil is in the opposite direction (with 180° phase difference) to the current in the *positive mode* Tx coil.
- 3) *Inactive mode* Tx: The output voltage of the inverter connected to this Tx is set to zero by activating two bottom switches at both legs on the full-bridge inverter. It is verified in the following analysis that the currents in the inactive Tx coil can be made insignificant in practical conditions. There are following two types of inactive coils: 1) *listening* mode ones that are waiting for an Rx to be presented and 2) *alert* mode ones adjacent to active

coils that are expecting an Rx to be moved on to them anytime.

Note that subscript i is used to denote the parameters related to the active Tx (*positive* mode or *negative* mode), and subscript k is used to denote the parameters related to *inactive* Tx throughout this article. The detailed description of activation and deactivation method is presented in Section V.

III. SYSTEM ANALYSIS

Next, let us analyze the characteristics of the system using the equivalent circuit method. The equivalent circuit analysis is carried out by using the fundamental-harmonic approximation. It is also assumed that all the Tx circuits are identical. The validity of these assumptions is experimentally verified in the following sections. The resonance frequency (ω_0) of each Tx and receiver circuits is defined as

$$\begin{aligned} \omega_0 &= \frac{1}{\sqrt{L_f C_f}} = \frac{1}{\sqrt{L_{Rx} C_{Rx}}} \\ &= \frac{1}{\sqrt{(L_{Tx} + \sum L_x - L_f) C_{Tx}}} \end{aligned} \quad (1)$$

where L_f , L_{Tx} , and L_{Rx} are the inductances of the compensation inductor, Tx coil, and Rx coil, respectively; and C_f , C_{Tx} , and C_{Rx} are the compensation capacitors used in the Tx and Rx circuits, as illustrated in Fig. 2. The effect of crosscoupling between the Tx coils (M_x) is compensated by coupled inductors whose individual inductance is L_x and mutual inductance is $-M_x$ (refer to Fig. 2). For simplicity, we use a single variable L_x to denote the inductance of the coupled inductor, however, they do not necessarily have to be identical.

A. Active Tx

The supply voltage for all the active Tx (either *positive* mode or *negative* mode) are set to have the same magnitude but either in-phase (defined as *positive* voltage) or out-of-phase (defined as *negative* voltage) depending on the activation mode of the Tx. The sign of the voltage source is defined as the same sign with the mutual coupling of its Tx coil and the Rx. In this way, the supply voltage $V_{s,i}$ at the fundamental working frequency ω_0 for the i th active Tx is defined as $V_{s,i} = \text{sign}[M_i]V_s$, where V_s is the voltage amplitude at frequency ω_0 , and M_i is the mutual inductance between the i th Tx coil and the receiver. Next, with the assumption of ideal lossless components, currents in the i th active (either *positive* or *negative* mode) Tx can be calculated as

$$I_{f,i} = \frac{M_{\text{sum}} M_i}{L_f^2} \frac{V_s}{R_L} \quad (2)$$

$$I_{Tx,i} = -\text{sign}[M_i] \frac{jV_s}{\omega_0 L_f} \quad (3)$$

where M_{sum} is the sum of mutual inductances between all the active Tx coils and the Rx coil, which can be defined as $M_{\text{sum}} = \sum_{p \in \mathcal{V}_i} |M_p|$.

Here, $I_{f,i}$ and $I_{Tx,i}$ are the currents through the compensation inductor L_f and the Tx coil L_{Tx} , respectively, and R_L is the load resistance. The input current of the active Tx $I_{f,i}$ is proportional

to M_i , which means when a receiver is moving away from an active Tx, the input current will decrease. This characteristic of the input current of the active Tx will assist the system to decide on turning OFF when receiver moves away from the charging area. Note that the Tx current amplitude is constant regardless of the mutual inductances (thus, for any Rx position) or the load resistance, while its phase is dependent on the sign of the mutual inductance (the negative sign represents 180° phase difference). In this way, *positive* or *negative* mode Tx coils can be realized by activating each inverter with the correct phase shift. With such activation, the currents in Rx I_{Rx} can be derived as

$$I_{\text{Rx}} = -\frac{M_{\text{sum}}}{L_f} \frac{V_s}{R_L} \quad (4)$$

and the voltage across the load resistance R_L becomes

$$V_L = -I_{\text{Rx}} R_L = \frac{M_{\text{sum}}}{L_f} V_s. \quad (5)$$

It can be observed that the load-independent voltage across the load is proportional to M_{sum} , that is, to the sum of all the mutual inductances between the active Tx coils and the Rx. With a proper coil design and correct activation of Tx coils, stable and position-independent voltage at the load can be realized if a stable M_{sum} is achieved at wide range of receiver positions.

B. Inactive Txs

As described earlier, the supply voltage is set to zero for *inactive* mode Tx circuits (refer to Fig. 2). With the assumption of ideal lossless components, inactive Tx coil current is completely nullified (i.e., $\bar{I}_{\text{Tx},k} = 0$) regardless of the receiver position.

However, in order to evaluate more realistic scenarios, the coil current of the k th inactive Tx coil $\bar{I}_{\text{Tx},k}$ is derived assuming a nonzero resistance R_f of the compensation inductor L_f . The result reads

$$\bar{I}_{\text{Tx},k} \approx j \frac{M_k R_f}{\omega_0 L_f^2 R_L} V_s \approx 0 \quad (6)$$

where M_k is the mutual inductance between the k th *inactive* Tx and the receiver. Note that a Tx coil will be deactivated when the receiver is far away from it because its mutual inductance with the receiver M_k is very small compared to L_f . Moreover, in typical WPT systems, the value of the resistance R_f is much smaller than $\omega_0 L_f R_L$. Therefore, *inactive* Tx coil currents will be very small in any realistic scenario. Now, it is clear from the abovementioned analysis that *inactive* Tx coils do not effectively produce any substantial electromagnetic field as their coil currents are insignificant. This is a remarkable and important feature of the proposed activation technique for large-area WPT because it will ensure safe operation without unwanted exposure.

Next, current in the compensation inductor (same as the input current branch when the Tx is in *active* mode) of the k th *inactive* Tx $\bar{I}_{f,k}$

$$\bar{I}_{f,k} = M_k \frac{V_s M_{\text{sum}}}{L_f^2 R_L}. \quad (7)$$

We see that it is directly proportional to M_k . Unlike *inactive* Tx coil currents, $\bar{I}_{f,k}$ can be substantially high if the value of the mutual inductance M_k is not extremely small. This feature can be used to identify if a receiver is close to an *inactive* Tx coil by measuring the current in L_f . The implementation of such detection method is discussed in Section V.

C. Performance Characteristics

Next, let us analyze the performance characteristics, including the output power P_{out} and the efficiency η . The number of *active* mode Txs for a given Rx position we denote by n . The output power is derived as

$$P_{\text{out}} = |I_{\text{Rx}}|^2 R_L = \left(\frac{M_{\text{sum}}}{L_f} \right)^2 \frac{V_s^2}{R_L}. \quad (8)$$

As discussed earlier, it is possible to ensure a stable output power for any receiver position if the sum of all the active mutual inductances M_{sum} is nearly constant regardless of the receiver position or orientation. Therefore, the design objective for achieving position-independent robust power transfer is to realize a stable M_{sum} .

The efficiency of the WPT link defined as the ratio of output power and total input power to the WPT system, which can be found as

$$\eta = \frac{1}{1 + \xi_{\text{Tx}} + \xi_x + \xi_f + \xi_{\text{Rx}}} \quad (9)$$

$$\xi_{\text{Tx}} = \frac{n R_{\text{Tx}} R_L}{(\omega_0 M_{\text{sum}})^2}, \quad \xi_x = \frac{n_x R_x R_L}{(\omega_0 M_{\text{sum}})^2}$$

$$\xi_f = \frac{R_f \left(\sum_{\forall i} M_i^2 + \sum_{\forall k} M_k^2 \right)}{R_L L_f^2}, \quad \xi_{\text{Rx}} = \frac{R_{\text{Rx}}}{R_L}$$

where $\xi_{\text{Tx},x,f,\text{Rx}}$ are the loss ratios in the Tx coil, the cross-coupling compensation inductor, the compensation inductor L_f , and the Rx coil, which are defined as the losses in the respective components relative to the power delivered to the load. The loss ratios in the Tx coils are proportional to the number of *active* mode Tx coils (n), therefore, the number of *active* mode Tx coils should be carefully optimized to achieve high efficiency. On the other hand, the loss ratio ξ_x is also proportional to the number of crosscoupling compensation inductors. However, in practice, the value of crosscoupling inductance is very small compared to the coil inductance, which results in a very small value for R_x resulting in comparatively smaller ξ_x . The losses in the Rx coil will be negligible if the Rx coil resistance is much smaller compared to the load resistance.

The losses in the compensation inductor L_f have two components, losses in *active* mode circuits and losses in *inactive* mode circuits. Nevertheless, we note that the losses in the *active* mode compensation inductor are inevitable in any design. The loss ratio contribution from *inactive* mode circuits is $(R_f \sum_{\forall k} M_k^2) / (R_L L_f^2)$, which is propositional to the sum of the mutual inductances between inactive Tx coils and the receiver. In fact, the mutual inductance of inactive coils is very small, therefore, the loss contribution from the *inactive* mode

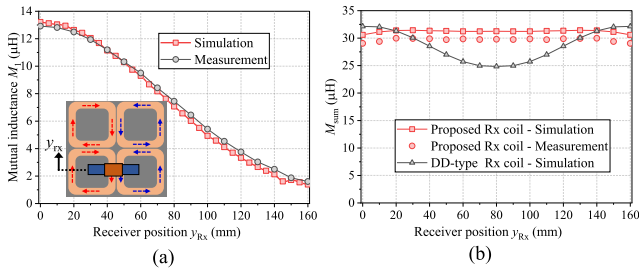


Fig. 3. (a) Simulated and measured mutual inductances between a single Tx (T_{x1}) and Rx with respect to the variation of the receiver position in y -direction (y_{Rx}). (b) M_{sum} variation of the proposed flux-pipe type receiver is compared with conventional DD-type receiver with the same dimensions and number of turns.

compensation inductor will be small. Ideally, inactive Tx coil currents are zero, not affecting efficiency. In practice, there will be very small currents, but the corresponding power loss is negligibly small.

IV. DESIGN AND THE EXPERIMENTAL PROTOTYPE

The design of the proposed coil configuration and the experimental prototype is next introduced in this section. First, the working frequency of the prototype WPT system is chosen as 200 kHz from practical considerations. However, in principle, the proposed concept is valid for an arbitrary frequency as long as the ferrite materials operate below the saturation at the maximum power level. In case if power level is too high, one may need to thicken the ferrite or use materials with higher saturation flux densities. For the construction of the WPT coils, 660/42-type Litz wire winding (i.e., the wire has 660 strands with the diameter of each strand equal to $60 \mu\text{m}$) is used. Simulations are carried out for the coil design, and the results are compared with classical DD-type Rx coils using COMSOL simulation tool.

A. Simulation and Comparison of the WPT Coils

The dimensions of the Tx and Rx coils are selected by considering the target application criteria of a mobile robot charging station. The transfer distance between the Tx array and the receiver (z_{Rx}) is chosen to be 50 mm. In order for Rx to couple with at least two adjacent Tx coils, the length of the Rx coil needs to be comparable with the diagonal of a single Tx coil. Therefore, the size of a single Tx coil is chosen as 15×15 cm and the size of the Rx coil is selected as 20×10 cm. The number of turns for the Tx coil and Rx coils are chosen to be 7 and 40, respectively. Higher number of turns is chosen for the Rx coil to achieve high mutual inductance.

The measured mutual inductance between a single Tx (T_{x1}) and Rx is compared with the simulation results with respect to the variation of the receiver position in the y -direction (y_{Rx}) in Fig. 3(a), and the measurements agree well with the simulations. It should be highlighted that the coil design is carried out for this specific configuration using the state-of-the-art knowledge on good engineering design. Coil optimizations for the proposed WPT topology could be further extended depending on the

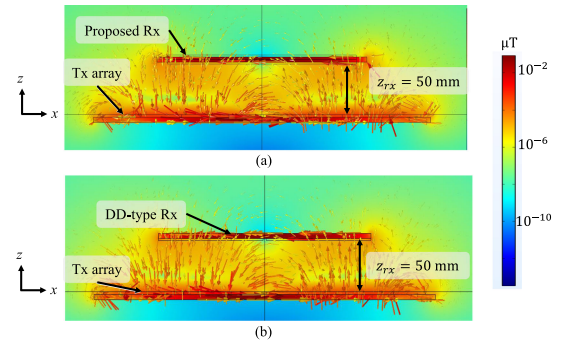


Fig. 4. Distribution of magnetic flux density of a four-Tx WPT system: Front view in the xz -plane at $y = 0$ (magnetic field vectors are shown with arrows), for (a) proposed receiver type and (b) classical DD-type receiver.

application criteria, such as different transfer distances and space constraints. Next, the mutual inductance variation of the proposed flux-pipe type receiver is compared with conventional DD-type receiver with the same dimensions and number of turns. Fig. 3(b) shows the comparison of the sum of mutual inductance (M_{sum}) variation of two types of the receiver with respect to the y -direction receiver position when four Tx coils are simultaneously activated. Here, all the geometric parameters and the number of turns are kept the same for both coil types. It can easily be observed that M_{sum} is more stable for the proposed flux-pipe Rx as compared to the DD-type.

Moving forward, the distribution of magnetic flux density of a four-Tx WPT system together with magnetic field vectors are shown in Fig. 4 for the proposed flux-pipe and classical DD-type Rx coils. It can be seen that the magnetic field lines from the *positive-mode* Tx coils go to the *negative-mode* Tx coils through the receiver ferrite core, as desired. It is important to observe from the field plots in Fig. 4 that both proposed Rx and classical DD-type Rx coils exhibit similar field distribution outside of the Rx coil. This means that the magnetic leakage of the proposed WPT system is comparable with the system with a DD-type Rx, therefore, known methods for magnetic shielding should work well with the proposed WPT system. Nevertheless, any WPT system would require proper magnetic shielding before commercial adaptation.

B. Experimental Prototype

The experimental validation of the proposed system is carried out by using a laboratory prototype of a six-Tx WPT system. The experimental setup is shown in Fig. 5. Full-bridge inverters are built using integrated gate drive GaN FET (*LMG5200*) and connected to Tx coils as the power sources through an LCC-tuned resonant circuit. A digital-signal-processor (DSP) (model no. *TI F28379D*) is used to generate the control signals for the full-bridge inverter switches. Due to the limitation of the number of signal channels in the DSP, three inverters are used to drive six Tx coils during the experimental tests. Multiple Tx coils are connected in parallel with the three converters to demonstrate different misalignment cases. Litz-wire winding and high-frequency

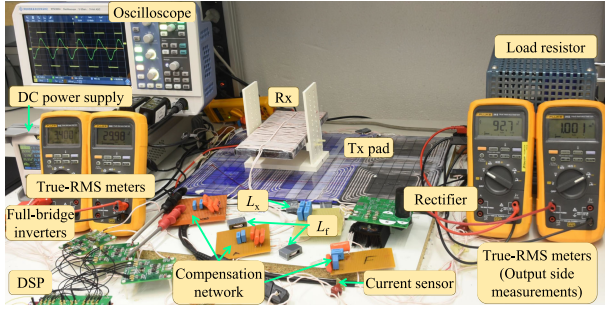


Fig. 5. Experimental setup.

TABLE I
DESIGN PARAMETERS OF THE WPT SYSTEM

Parameter	value
Resonance frequency $f_0 = \omega_0/(2\pi)$	200 kHz
Input DC voltage V_{DC}	30 V
Transfer distance z_{Rx}	50 mm
Tx Inductance (L_{Tx})	16 μ H
Tx coil quality factor (Q_{Tx})	583
Rx Inductance (L_{Rx})	266 μ H
Rx coil quality factor (Q_{Rx})	588
Compensation inductor L_f	9.4 μ H
Cross coupling M_x	0.25 – 1.2 μ H
Coupling coefficient k	0.2 – 0.03

ferrite plates (type *TDK-PC95*) are used to construct WPT coils. Tx and Rx coils have a 1.5 mm gap between the turns to achieve low proximity-effect resistance [28]. Compensation inductors and crosscoupling compensator inductors are made using *N97* type ferrite ETD-cores, see Fig. 5. The design parameters of the WPT system are listed in Table I. The nominal transfer distance of 50 mm is chosen for the experimental study. Note that Rx inductance is considerably higher than Tx inductance due to the different coil types and number of turns. For the measurement of the output power and efficiency, the dc voltages and currents are measured with high-accuracy industrial grade true-RMS meters (model *FLUKE 28 II*).

V. RECEIVER DETECTION AND TX ACTIVATION

A. Proposed Activation Method

The receiver detection and Tx activation method is systematically presented in this section. The proposed activation method is based on the concept of sensing the receiver position by using its induced effects in adjacent inactive Tx coils. As discussed in Section III-B, the inactive Tx input current $\bar{I}_{f,k}$ is proportional to the mutual inductance M_k between the inactive Tx and the Rx. This means that $\bar{I}_{f,k}$ becomes significantly high when there is an Rx nearby the inactive Tx. This property is exploited for the proposed receiver detection and activation method.

Fig. 6 illustrates the logic flow of receiver detection and the Tx activation method. Three modes have been defined namely, *listening*, *active*, and *alert*. At first, when the system is turned ON, it goes to the *listening* mode where a set of Txs are activated in a selected pattern (for example, the check-box pattern) periodically for a short time, while the rest of the Txs are kept turned OFF. Then, the input current of the inactive Tx $\bar{I}_{f,k}$ is measured

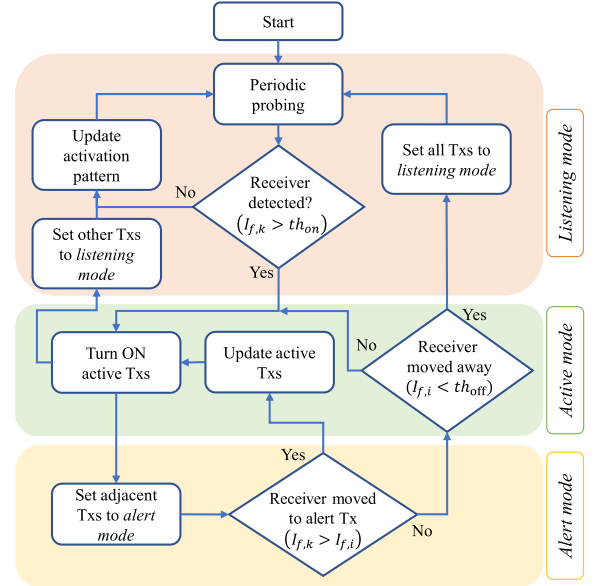


Fig. 6. Flowchart of the proposed Tx activation/deactivation.

to determine whether there is an Rx present. If $\bar{I}_{f,k}$ is very small (lower than the threshold th_{on} determined by practical noise level), it means that there is no receiver in the vicinity. Then, the system updates the pattern of the Tx to be activated in the next periodic check. At any moment when there is a receiver between an active coil and an inactive coil, the inactive Tx's $\bar{I}_{f,k}$ will be higher than the turn-ON threshold th_{on} . The phase of the inactive current with respect to the supply voltage of the active Tx defines the sign of the mutual inductances between the active-Tx and Rx (M_i), and inactive-Tx and Rx (M_k) are of the same sign, otherwise, if they are out-of-phase, the two mutual inductances have the opposite signs, as seen from (7). Then, all the Txs with $\bar{I}_{f,k}$ higher than the turn-ON threshold th_{on} will be activated with the proper phase, i.e., Txs with the same mutual inductances polarities are activated with synchronized supply voltages.

When a receiver is moving within the charging area, the activation of the Tx coils should be updated to trace the Rx position. To this end, when a receiver is detected, the Txs adjacent to the active Tx coils are set to the *alert* mode. The *alert* mode coils are expecting the receiver to be moved toward it at any time. All the other Txs in the Tx pad will remain in the *listening* mode. The Txs in the *alert* mode will keep comparing their inactive input current $\bar{I}_{f,k}$ with the active coil input current $I_{f,i}$. At any moment, when a receiver is moving toward a particular *alert*-Tx, $\bar{I}_{f,k}$ of that Tx will be higher than the input current of the active coil to be turned OFF [compare (2) and (7)]. Then, the system will update the active Txs accordingly. As long as the *alert*-Tx's input current is lower than the active-coil input current they remain in the *alert* mode.

Next, it should be possible to detect if the receiver completely moves away from the charging area to turn OFF all the active coils. For making the turn-OFF decision, we use the property of (2) that the input current of the active coils is proportional to M_{sum} . When the Rx is far from all active coils, the value

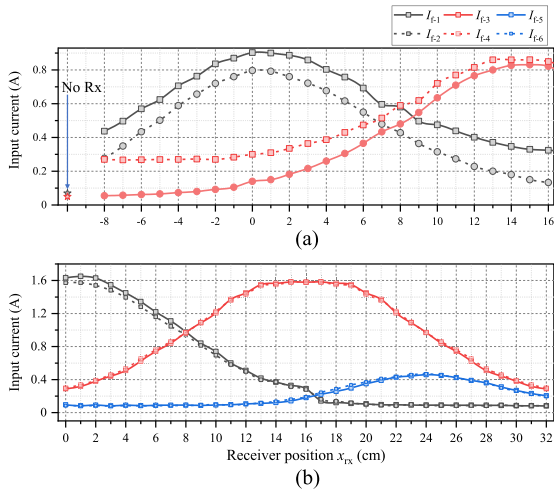


Fig. 7. Input current of the active and inactive Tx coils.

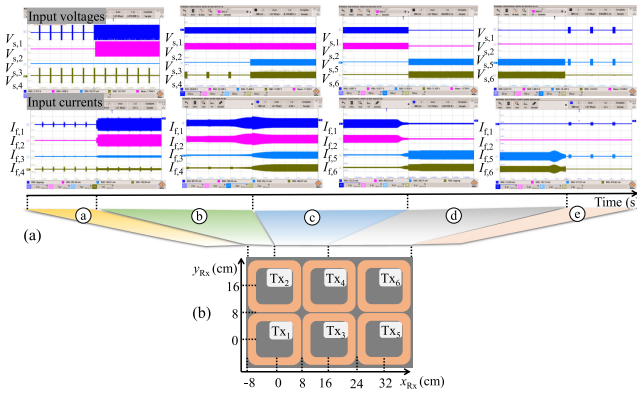


Fig. 8. Experimental waveforms during the receiver movement across the Tx pad with the proposed dynamic activation of the Tx coils.

of M_{sum} will be very low leading to low-input currents in the active coils. Therefore, the value of the input current of active Tx coils $I_{f,i}$ are compared with the turn-OFF threshold th_{off} . Note that the threshold th_{off} needs to be determined experimentally based on $I_{f,i}$ of the active Tx coils without the Rx because higher order harmonics of the input current could be dominant in that situation.

B. Validation of Tx Activation

In order to verify the proposed activation method, experiments are conducted using six Tx coils [the test configuration and the coordinate system is illustrated in Fig. 8(b)]. To depict the *listening* mode and the *alert* mode of the system, two separate tests are performed. For demonstrating the *listening* mode, $Tx_{1,4}$ are activated while $Tx_{2,3,5,6}$ are kept inactive and the currents in Tx_{1-4} are measured while the Rx is moved along the x -direction. Tx coils are not dynamically activated/deactivated during these initial tests. Fig. 7(a) shows the measured RMS currents. First, when the Rx is outside of the Tx pad area, all the active and

inactive currents are very low [indicated with a star in Fig. 7(a)], whereas when the Rx is moving on to the pad at $x_{rx} = -8$ cm, the input current in both active (Tx_1) and inactive (Tx_2) Tx coils start to grow. Compared to the case where there is no receiver on the pad, the input current in inactive Tx (i.e., $I_{f,2}$) shows a significant increase whenever the receiver comes onto a Tx coil (in between Tx_1 and Tx_2). Here, we set the threshold th_{on} as 150 mA to avoid false turn-ON due to measurement noise. Therefore, when the Rx reaches $x_{rx} = -7$ cm, $Tx_{1,2}$ will turn ON and $Tx_{3,4}$ will turn ON when the receiver position crosses the origin at $x_{rx} = 0$.

Next, when four Tx coils (Tx_{1-4}) are activated, other two adjacent Tx coils ($Tx_{5,6}$) are in *alert* mode. To demonstrate the working principle of the *alert* mode, Fig. 7(b) shows the measured input RMS currents in all six coils when Tx_{1-4} are active and $Tx_{5,6}$ are inactive. When the mutual inductance between any active-Tx and Rx is lower than the mutual inductance between an *alert* mode Tx and Rx, that particular *alert* mode Tx should be turned ON. This is detected by comparing input currents in *active* Tx coils and *alert* Tx coils. It can be clearly observed from Fig. 7(b) that the transition correctly happens at around $x_{rx} = 16$ cm (i.e., $I_{f,1}$ and $I_{f,2} > I_{f,5}$ and $I_{f,6}$).

The detection of receiver moving away from the Tx pad can be demonstrated by observing the input currents of active Tx coils (i.e., $I_{f,1}$ and $I_{f,2}$) in Fig. 7(b) where the input currents in the active Tx coils Tx_{1-2} drop down to 120 mA when the receiver is not present (e.g., when $x_{rx} > 20$ cm). Here, we set the threshold th_{off} to be 150 mA.

Finally, to validate dynamic activation during the operating conditions, we move the Rx across the Tx pad in x -direction and the coils are activated/deactivated automatically on the move. Input voltages and currents are recorded, as shown in Fig. 8. The three modes, *listening*, *active*, and *alert* are shown in Fig. 8 by different Rx position segments (a)–(e).

In segment (a), when the Rx is outside the Tx pad, the system is in the *listening* mode where Tx_1 and Tx_4 are periodically turned-ON and the rest are inactive. When the Rx moves to segment (b), the Rx comes on top of $Tx_{1,2}$, therefore, two Tx coils are turned ON. However, the Rx is still away from $Tx_{3,4}$, therefore, it remains inactive. When the Rx moves to (c), Tx_{1-4} are activated, and $Tx_{5,6}$ are changed to the *alert* mode. Next, at the segment (d), the Rx moves toward *alert* $Tx_{5,6}$, which will activate those and switch $Tx_{1,2}$ to the *listening* mode. Finally, when the Rx is moving away from the Tx pad (e), all the active Tx coils are turned OFF and the whole system switches back to *listening* mode. To summarize, the proposed activation method is successfully demonstrated for the receiver movement across the Tx pad.

It should be noted that the demonstration of the abovementioned cases have been done in three sets of experimental tests due to the limitation of the number of inverters in our experimental prototype. However, in actual implementations, all the Tx circuits can be made modular with a central processor sending control signals. In fact, even in practical situations with many Tx coils, it is not necessary to measure the currents in all the Tx circuits. For example, a receiver tracking and trajectory planning

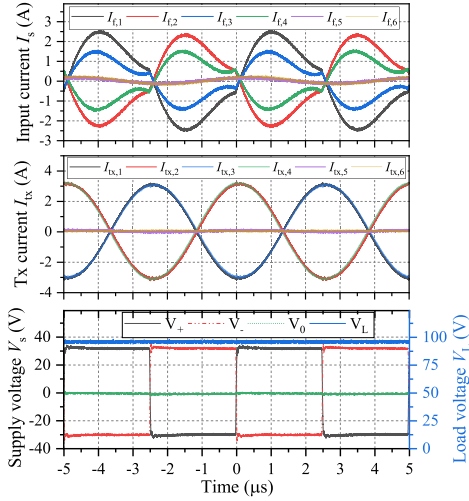


Fig. 9. Experimental waveforms of the input current, Tx coil currents, supply voltage, and load voltage when the receiver is at $x_{rx} = 6$ cm and $y_{rx} = 8$ cm.

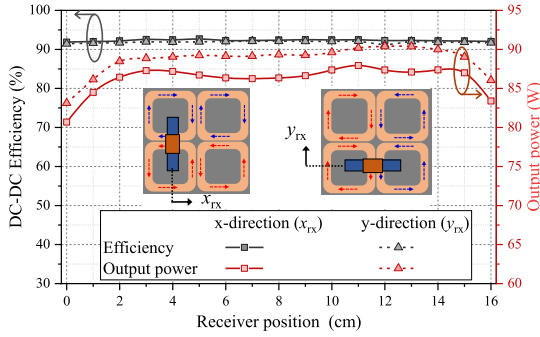


Fig. 10. Variation of the output power and efficiency with respect to the receiver movement in the x - and y -directions.

algorithm can be developed using machine learning algorithms so that the position sensing does not interrupt the continuous power transfer to the receiver.

VI. EXPERIMENTAL RESULTS

The performance variations of the laboratory prototype with respect to different misalignment conditions are presented in this section. The performances are evaluated at different Rx positions across the Tx pad when four Tx coils are activated. The experimental waveforms of the input currents, Tx coil currents, supply voltage, and load voltage are given in Fig. 9 for the receiver position at $x_{rx} = 6$ cm and $y_{rx} = 8$ cm. It can be observed that inactive-Tx-coil currents are almost zero.

A. Experimental Verification

First, the performances are measured with respect to receiver movements in the x - and y -directions when there are four active Tx coils, as illustrated in Fig. 10.

The measured maximum efficiency (from dc power source to dc load resistance) is 91% with only 1% variation for all receiver

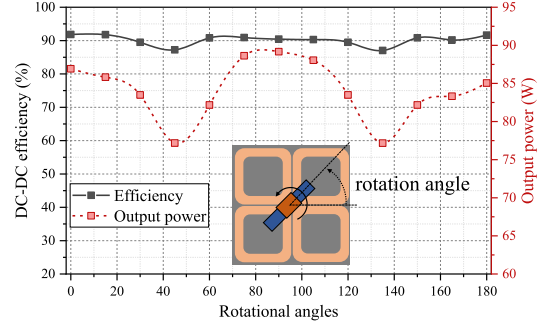


Fig. 11. Variation of the experimentally measured total efficiency and output power against receiver's rotation angle.

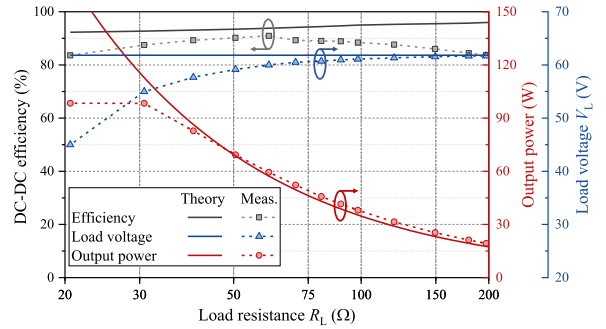


Fig. 12. Comparison of the experimental performance with the theoretical calculations with respect to the load resistance.

positions along x - and y -directional movement. Furthermore, the power received by the load is relatively stable against receiver movements at the center of the Tx pad. This power profile is inline with M_{sum} profile in Fig. 3.

Next, the experiments are performed while the Rx is rotated around its axis at the center of the four active Tx's. From the results presented in Fig. 11, it is clear that the total efficiency is still around 90% regardless of the rotation angle. However, we observe a slight drop in the received power at certain angles, which is anyway inevitable also in any classical WPT realization.

Finally, the WPT performance is evaluated against different load resistance values. The results, given in Fig. 12, verify that the proposed WPT configuration exhibits robust performance with the output voltage variations smaller than 5 V for the load values higher than 40 Ω (note that the dc supply voltage is kept at 20 V for this test to keep the power level within the rated power of the inverter). For low-load-resistance values, the output voltage drops from the theoretical value, however, the efficiency is still maintained higher than 85%. This drop of the voltage at lower load resistance values is attributed to the losses in the receiver coil and rectifier, and to the effect of a slight detuning of the Rx coil at low load resistance values.

B. Asymmetric Misalignment Conditions

The experimental study is then continued to portray the robustness of the proposed system at different misalignment conditions. To this end, the receiver is moved along several

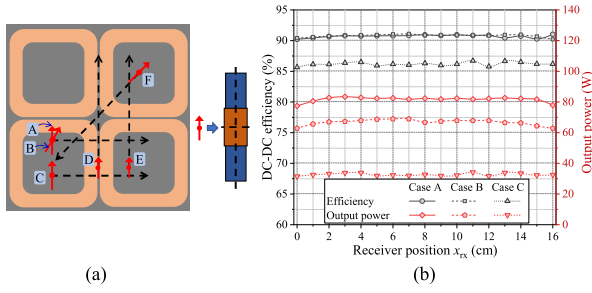


Fig. 13. (a) Different misalignment cases. Rx movement in; Case A – x -direction at $y_{rx}=6$ cm, Case B – x -direction at $y_{rx}=6$ cm with an angular misalignment of 15° , Case C – x -direction at $y_{rx}=2$ cm, Case D – y -direction at $x_{rx}=8$ cm with Rx orientation in y -direction, Case E – y -direction at $x_{rx}=12$ cm with Rx orientation in y -direction, Case F – diagonal direction from with an angular misalignment of 45° . (b) The performance variations for Cases A, B, and C.

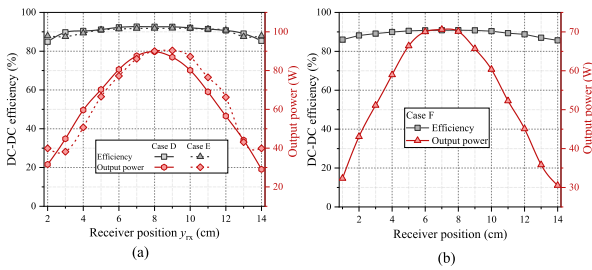


Fig. 14. Performance variation against asymmetric misalignment for the (a) receiver movement in y -direction (i.e., Case D and Case E) and (b) receiver movement in the diagonal direction (i.e., Case F).

asymmetrically misaligned paths as shown in Fig. 13(a) (the details of different paths are given in figure caption). Fig. 13(b) shows the performance variations when the receiver moves along the paths A, B, and C. The efficiency is more than 90% and the output power is between 60 and 85 W for cases A and B, respectively. Note that case B corresponds to the same movement as Case A but with a 15° angular rotation. Case C depicts an extreme misalignment situation, when Rx moves at the edge of the Tx pad. Even at this extreme case, the total efficiency is still around 86%–87% and the output power is around 40 W. Interestingly, the movement along the x -direction does not degrade the performances in all the three cases. Next, for Cases D and E, the Rx is moved along the y -direction, while its orientation along the same direction is fixed. It can be seen from Fig. 14(a) that efficiency is around 90% for these cases as well. The drop in the output power when the Rx is at the edge of the Tx pad is due to the same reason as explained above. Finally, for Case F, the Rx is moved diagonally with an angle of 45° , as illustrated in Fig. 13(a). It can be seen from the results in Fig. 14(b) that efficiency is between 86% and 91%.

Therefore, it is clear that the proposed WPT system demonstrate fairly high-efficiency at full range of different misalignment conditions. On the other hand, although power drops when the Rx moves to the edge of the Tx pad, the power profile is stable for most of the Rx movements within the Tx pad. This power drop at extreme positions is inevitable in any WPT system with a fixed supply voltage. This issue can be solved by using adaptive tuning methods by adjusting the input voltage. Note that the

efficiency of the system will still be high even with a drop in the output power. Therefore, in certain applications, it may be not even necessary to regulate it. For example, in a battery charging application, the battery may still be charged with a lower power level, but fully and efficiently.

Finally, let us make a few remarks on the general applicability of the proposed WPT topology. First, the compensation topology that can be used in this configuration is not limited to the LCC–S type, and different compensation typologies can be applied. For example, LCC–type compensation can be used also at the Rx side (i.e., LCC–LCC) to enable constant-current characteristics at the receiver [29]. Second, different Rx coil configurations other than the flux-pipe type proposed in this article can be used along with a proper optimization. For example, Rx coils of DD type or cross-dipole Rx coils can also be used, depending on the application criteria. Third, the Tx coil configuration can also be optimized for different dimensions and shapes. One interesting possibility is to test hexagonal coils for the Tx pad. Forth, the proposed WPT configuration can also be applied to free-positioning WPT to multiple receivers. As long as the coupling between multiple Rx coils is negligible, the theoretical analysis is valid also for multiple receivers. In addition, the proposed method can be used from low-power to high-power applications without any principal modifications. At high power, optimization of coils may be needed with the goal to keep magnetic materials within their saturation levels. Finally, the continuation of the proposed WPT system with a commercial application would require electromagnetic leakage testing with a design of proper shielding methods similar to any other WPT system.

VII. CONCLUSION

This article proposed an efficient WPT system to enable wireless charging in a large area that can be applied for wireless charging of movable electric devices, such as automated robots or drones. The introduced coil configuration consisted of multiple square-shaped coils with a ferrite layer as Tx coils and an Rx coil wound around a ferrite core. This new configurable multi-Tx WPT system generated almost continuous electromagnetic flux path from a set of Tx coils to another set of Tx coils through the receiver coil ferrite core regardless of the receiver position or orientation, which ensured efficient power transfer over the whole charging area. A novel method was proposed to detect the position and orientation of the receiver based on the observation of the input current in the compensating inductor for the inactive Tx coils. The working principle and the operation of the proposed method were rigorously analyzed and experimentally verified. The experimental results showed dc-to-dc efficiency higher than 90% most of the receiver position or orientation. Even though there can be a drop in output power at extreme Rx positions, the efficiency is always higher than 85% even at extreme Rx positions.

ACKNOWLEDGMENT

The authors would like to thank Professor Sergei Tretyakov for the guidance and useful discussions.

REFERENCES

- [1] J. Yin, D. Lin, C. K. Lee, T. Parisini, and S. Y. Hui, "Front-end monitoring of multiple loads in wireless power transfer systems without wireless communication systems," *IEEE Trans. Power Electron.*, vol. 31, no. 3, pp. 2510–2517, Mar. 2016.
- [2] S. Li and C. C. Mi, "Wireless power transfer for electric vehicle applications," *IEEE J. Emerg. Sel. Topics Power Electron.*, vol. 3, no. 1, pp. 4–17, Mar. 2015.
- [3] M. Tampubolon, L. Pamungkas, H.-J. Chiu, Y.-C. Liu, and Y.-C. Hsieh, "Dynamic wireless power transfer for logistic robots," *Energies*, vol. 11, Feb. 2018, Art. no. 527.
- [4] J. Li and H. Liu, "Design optimization of Amazon robotics," *Automat., Control Intell. Syst.*, vol. 4, no. 2, pp. 48–52, 2016.
- [5] C. C. Mi, G. Buja, S. Y. Choi, and C. T. Rim, "Modern advances in wireless power transfer systems for roadway powered electric vehicles," *IEEE Trans. Ind. Electron.*, vol. 63, no. 10, pp. 6533–6545, Oct. 2016.
- [6] J. Shin *et al.*, "Design and implementation of shaped magnetic-resonance-based wireless power transfer system for roadway-powered moving electric vehicles," *IEEE Trans. Ind. Electron.*, vol. 61, no. 3, pp. 1179–1192, Mar. 2014.
- [7] P. K. S. Jayathurathnage, A. Alphones, D. M. Vilathgamuwa, and A. Ong, "Optimum transmitter current distribution for dynamic wireless power transfer with segmented array," *IEEE Trans. Microw. Theory Techn.*, vol. 66, no. 1, pp. 346–356, Jan. 2018.
- [8] D. Kim and D. Ahn, "Maximum efficiency point tracking for multiple-transmitter wireless power transfer," *IEEE Trans. Power Electron.*, vol. 35, no. 11, pp. 11391–11400, Nov. 2020.
- [9] W. Kim and D. Ahn, "Efficient deactivation of unused LCC inverter for multiple transmitter wireless power transfer," *IET Power Electron.*, vol. 12, no. 1, pp. 72–82, 2019.
- [10] F. Lu, H. Zhang, H. Hofmann, and C. C. Mi, "A dynamic charging system with reduced output power pulsation for electric vehicles," *IEEE Trans. Ind. Electron.*, vol. 63, no. 10, pp. 6580–6590, Oct. 2016.
- [11] T. Kan, T. Nguyen, J. C. White, R. K. Malhan, and C. C. Mi, "A new integration method for an electric vehicle wireless charging system using LCC compensation topology: Analysis and design," *IEEE Trans. Power Electron.*, vol. 32, no. 2, pp. 1638–1650, Feb. 2017.
- [12] C. Park, S. Lee, S. Y. Jeong, G. Cho, and C. T. Rim, "Uniform power I-type inductive power transfer system with DQ-power supply rails for on-line electric vehicles," *IEEE Trans. Power Electron.*, vol. 30, no. 11, pp. 6446–6455, Nov. 2015.
- [13] S. Song, Q. Zhang, Z. He, H. Li, and X. Zhang, "Uniform power dynamic wireless charging system with I-type power supply rail and DQ-phase-receiver employing receiver-side control," *IEEE Trans. Power Electron.*, vol. 35, no. 10, pp. 11205–11212, Oct. 2020.
- [14] Y. Li *et al.*, "A new coil structure and its optimization design with constant output voltage and constant output current for electric vehicle dynamic wireless charging," *IEEE Trans. Ind. Informat.*, vol. 15, no. 9, pp. 5244–5256, Sep. 2019.
- [15] F. Farajzadeh, D. M. Vilathgamuwa, D. Jovanovic, P. Jayathurathnage, G. Ledwich, and U. Madawala, "Expandable N-legged converter to drive closely spaced multitransmitter wireless power transfer systems for dynamic charging," *IEEE Trans. Power Electron.*, vol. 35, no. 4, pp. 3794–3806, Apr. 2020.
- [16] M. Budhia, J. T. Boys, G. A. Covic, and C. Huang, "Development of a single-sided flux magnetic coupler for electric vehicle IPT charging systems," *IEEE Trans. Ind. Electron.*, vol. 60, no. 1, pp. 318–328, Jan. 2013.
- [17] M. Budhia, G. A. Covic, J. T. Boys, and C. Huang, "Development and evaluation of single sided flux couplers for contactless electric vehicle charging," in *Proc. IEEE Energy Convers. Congr. Expo.*, 2011, pp. 614–621.
- [18] X. Zhang, Y. Zhang, Z. Zhang, and M. Li, "Mode conversion and structure optimization of quadrature coils for electric vehicles wireless power transfer," *IEEE Trans. Energy Convers.*, vol. 35, no. 2, pp. 575–590, Jun. 2020.
- [19] Q. Xu, H. Wang, Z. Gao, Z. Mao, J. He, and M. Sun, "A novel mat-based system for position-varying wireless power transfer to biomedical implants," *IEEE Trans. Magn.*, vol. 49, no. 8, pp. 4774–4779, Aug. 2013.
- [20] Z. Zhang and K. T. Chau, "Homogeneous wireless power transfer for move-and-charge," *IEEE Trans. Power Electron.*, vol. 30, no. 11, pp. 6213–6220, Nov. 2015.
- [21] D. Kobayashi, T. Imura, and Y. Hori, "Real-time coupling coefficient estimation and maximum efficiency control on dynamic wireless power transfer for electric vehicles," in *Proc. IEEE PELS Workshop Emerg. Technol.: Wireless Power*, 2015, pp. 1–6.
- [22] X. Dai, X. Li, Y. Li, and A. P. Hu, "Maximum efficiency tracking for wireless power transfer systems with dynamic coupling coefficient estimation," *IEEE Trans. Power Electron.*, vol. 33, no. 6, pp. 5005–5015, Jun. 2018.
- [23] D. Kim, S. Kim, S. Kim, J. Moon, I. Cho, and D. Ahn, "Coupling extraction and maximum efficiency tracking for multiple concurrent transmitters in dynamic wireless charging," *IEEE Trans. Power Electron.*, vol. 35, no. 8, pp. 7853–7862, Aug. 2020.
- [24] A. N. Azad, A. Echols, V. A. Kulyukin, R. Zane, and Z. Pantic, "Analysis, optimization, and demonstration of a vehicular detection system intended for dynamic wireless charging applications," *IEEE Trans. Transport. Electrification*, vol. 5, no. 1, pp. 147–161, Mar. 2019.
- [25] X. Meng, D. Qiu, M. Lin, S. TangChun, and B. Zhang, "Output voltage identification based on transmitting side information for implantable wireless power transfer system," *IEEE Access*, vol. 7, pp. 2938–2946, 2019.
- [26] S. Mukherjee *et al.*, "Control of output power in primary side LCC and secondary series tuned wireless power transfer system without secondary side sensors," in *Proc. IEEE Energy Convers. Congr. Expo.*, 2020, pp. 5532–5536.
- [27] Y. Liu, U. K. Madawala, R. Mai, and Z. He, "Primary-side parameter estimation method for bidirectional inductive power transfer systems," *IEEE Trans. Power Electron.*, vol. 36, no. 1, pp. 68–72, Jan. 2021.
- [28] J. Kim and Y.-J. Park, "Approximate closed-form formula for calculating ohmic resistance in coils of parallel round wires with unequal pitches," *IEEE Trans. Ind. Electron.*, vol. 62, no. 6, pp. 3482–3489, Jun. 2015.
- [29] S. Li, W. Li, J. Deng, T. D. Nguyen, and C. C. Mi, "A double-sided LCC compensation network and its tuning method for wireless power transfer," *IEEE Trans. Veh. Technol.*, vol. 64, no. 6, pp. 2261–2273, Jun. 2015.



Shamsul Arefeen Al Mahmud received the B.Sc. degree in electrical engineering from United International University, Dhaka, Bangladesh, in 2015, and the M.Sc. degree in autonomous systems from Aalto University, Espoo, Finland, and the KTH Royal Institute of Technology, Stockholm, Sweden, in 2020. He is currently working toward the doctoral degree in electrical engineering with the Department of Electronics and Nanoengineering, School of Electrical Engineering, Aalto University.

His research interests include electronics and wireless power transfer systems.



Ishtiaque Panhwar received the B.Sc. degree in electrical engineering from the Mehran University of Engineering and Technology, Jamshoro, Pakistan, in 2015, and the M.Sc. degree in automation and electrical engineering from Aalto University, Espoo, Finland, in 2021.

He is currently a Researcher with the School of Electrical Engineering, Aalto University. His research interests include power electronics and wireless power transfer systems.



Prasad Jayathurathnage (Member, IEEE) received the B.Sc. degree in electronics and telecommunications engineering from the University of Moratuwa, Moratuwa, Sri Lanka, in 2009, and the Ph.D. degree in electrical and electronic engineering from Nanyang Technological University, Singapore, in 2017.

He has been with the Queensland University of Technology, Brisbane, QLD, Australia, in 2016, and Rolls-Royce-NTU Corporate Lab, Singapore, in 2017. He is currently a Postdoctoral Researcher with the School of Electrical Engineering, Aalto University, Espoo, Finland. His research interests include high-frequency power converters, wide-band-gap devices, and wireless power transfer.